(2)

LASER SPECTROSCOPY OF QUANTUM WELL AND SUPERLATTICE STRUCTURES

By

PROFESSOR B. HENDERSON

Department of Physics and Applied Physics,
University of Strathclyde,
John Anderson Building,
107 Rottenrow,
Glasgow G4 ONG,
Scotland.

Final Technical Report
4th June, 1990 - 3rd February, 1991.

Contract Number: DAJA45-88-C-0006
Red. No 5782-EE-01

The research reported in this document has been made possible through the support and sponsorship of the U.S. Government through the European Research Office of the U.S. Army. This report is intended only for the internal management use of the Contractor and the U.S. Government.

A. INTRODUCTION

The potential for tailoring band structures of semiconductors with specific properties using molecular beam epitaxy (MBE) and metallorganic chemical vapour deposition (MOCVD) has considerable significance for future electronic and optoelectronic devices. These techniques permit the growth of structures with alternating layers of two semiconductors on top of each other (Fig. 1a), which have band structures that alternate with characteristic peridocity (Fib. 1b) giving a one-dimensional Kronig-Penney structure. Superlattices are grown with well widths ranging from 1-50nm with rather thicker barriers. Electrons and holes are confined in the potential wells in the conduction and valence bands respectively. For a one-dimensional potential well the approximate eigenvalues are

$$E^n = \frac{h^2}{8m^*}\left[\frac{(n-\alpha)^2}{L_z^2}\right] \qquad (1)$$

yielding confinement energies E^n_{cb} and E^n_{vb} which depend on the quantum defect α, effective mass m^* and well width, L_z. Optical transitions across the smaller bandgap, subject to the selection rule $\Delta n=0$ occur at photon energies

$$\frac{hc}{\lambda_n} = \Delta_G + (E^n_{cb} + E^n_{vb})$$

$$= \Delta_G + \frac{n^2h^2}{8L_z^2}\left(\frac{1}{m^*_e} + \frac{1}{m^*_h}\right) \qquad (2)$$

(ignoring effects due to quantum defects). In view of the valence band splitting and the different effective masses in the two sub-bands there are two absorption transitions for each particular n-value. The effect is illustrated in Fig. 1c. However, because of the very fast energy relaxation of electrons and holes within the bands the only photoluminescence spectrum observed at low temperatures is that due to the lowest energy n=1 absorption band.

In general, the transition rates of these excitonic luminescence processes should be given by the inverse of the radiative lifetime, τ_R, leading to an homogeneous linewidth $\Delta\omega = (\tau_R)^{-1}$. At low temperature the exciton linewidth for a typical 5.0nm well in GaAs is about 100 times larger than in bulk material, which is already inhomogeneously broadened by the effects of strain. Obviously the exciton luminescence line experiences an additional inhomogeneous broadening which dominates the experimental linewidth. In GaAs

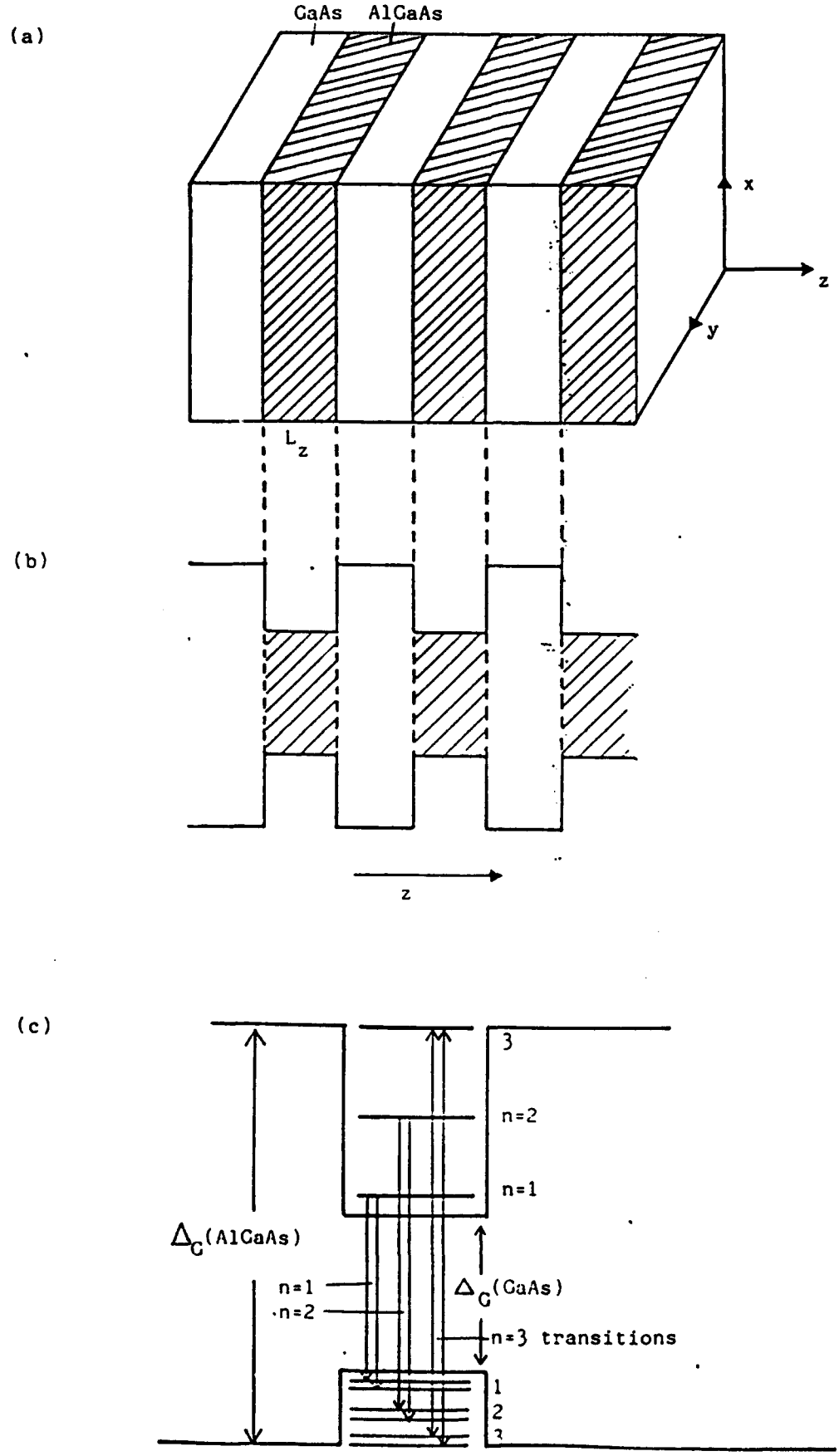

Figure 1. (a) Schematic of alternating thin layers of GaAs/AlGaAs in a MQWS, (b) modulation of the band structure of a MQWS in (a) and (c) allowed ($\Delta n=0$) optical transitions of MQWS.

the quantum well exciton is an optical probe approximately 20nm across which samples details of the environment in which it decays. This sampling yields, through the photon energy and measurements of homogeneous versus inhomogeneous width, detailed information about the broadening process. One obvious contribution is the variation in the width of individual wells present in a sample which contains up to 50 individual well/barrier periods grown sequentially. Another source of strain is the difference in unit cell dimensions of the two materials. This strain is accommodated elastically in very thin layers if the mismatch is large, and in relatively thick layers when the mismatch is small. Multi-quantum well structures (MQWS) based on the GaAs/AlGaAs system are said to be 'lattice-matched': the mismatch strain is very small and there is no loss of registry of lattice planes across the GaAs/AlGaAs interface. The lattice mismatch is much larger in GaAs/InGaAs: when thin epistructures of this system are grown without dislocations being nucleated at the GaAs/InGaAs interface 'strained layer superlattices' (SLSs) result. Other device-related SLSs are grown from the Zn(Cd)S(Se) family of semiconductors and from Si/Si_xGe_{1-x} materials. The former has possible applications in optoelectronics for the visible region and the latter in devices for optical communications.

Piezoelectric fields are generated when crystals lacking inversion symmetry are elastically deformed. In cubic crystals the piezoelectric effect requires a shear deformation such as that which results when strained layer superlattices are grown on (111) oriented substrates. This effect can alter the optical properties of group III-V and group II-VI semiconductors [1]. Indeed, there are significant differences between the optical properties of InGaAs-GaAs and CdS-CdSe strained layer superlattices grown on (111) and (100) substrates [2,3]. On the other hand, no significant differences are found for *lattice-matched* III-V superlattices grown on differently oriented substates [4]. In certain II-VI compounds, there exists the possibility of growing hexagonal (wurtzite) epilayers on (111) cubic substrates [3]. An example of a wurtzite strained layer superlattice, is the CdS-CdSe system grown on (111)A GaAs substrates [5,6]. Time- dependent optical effects due to screening of giant piezoelectric fields by photoexcited carriers are observed in these superlattices. CdS/CdSe hexagonal superlattices are ideal to observe such effects because the relevant piezoelectric coefficients are about three times larger than in cubic III-V compounds. Furthermore, the lattice mismatch between wurtzite CdS and CdSe is very large (5%) and the carrier lifetime is reasonably short.

B. AIMS OF PRESENT STUDIES AND MATERIALS

The intent of this experimental study was to study the inhomogeneous broadening of excitonic transitions using the techniques of :-

i) excitation and fluorescence spectroscopy,
ii) fluorescence line narrowing,
iii)radiative decay and time-resolved luminescence, and
iv) magneto-optic spectroscopy including optically detected magnetic resonance

The different samples studied included a range of single epilayers of $Al_xGa_{1-x}As$ grown on semi-insulating GaAs substrates obtained from the Plessey Company. The epilayers were doped with ca $2x10^{17}cm^{-3}$ Zn-acceptors. Two $GaAs/Al_xGa_{1-x}As$ MQWs were grown on (100) GaAs substrates at Philips Research Labs. (Redhill, U.K.). KLB155 comprised 20 monolayers of undoped GaAs with thickness 5.5nm alternated with $Al_{0.35}Ga_{0.65}As$ barriers with thickness 13.5nm, whereas KLB219 comprised 60 monolayers of 6.0nm thick GaAs separated by 17.5nm thick $Al_{0.35}Ga_{0.65}As$ barriers. Prof. C. Stanley of the University of Glasgow grew one multiple-single quantum well sample GUS154 consisting of 3 GaAs wells with thicknesses 4.0nm, 7.0nm and 11.0nm separated by 1.60nm $Ga_{0.6}Al_{0.4}As$ barriers grown on an ultrapure GaAs substrate traceable to RSRE (Malvern). Other GaAs/AlGaAs epistructures were provided by Dr J. Zavada of the E.R.O. Chalcogenide superlattices were grown on GaAs substrates at RSRE (Malvern) by the author's Research student, Mr P. J. Parbrook [7,8]. The well and barrier layer thicknesses were measured using X-ray diffraction and electron microscopy. The following typical samples were studied in detail :

ZP181: 100 periods of 5.2nm/0.6nm ZnS/ZnSe on (100) GaAs without buffer;
MH121: 20 periods of 2.5nm/2.5nm CdS/CdSe on (111)A GaAs with CdS buffer;
ZP247: 100 periods of 5nm/1.0nm ZnSe/CdSe on (100) GaAs with ZnSe buffer;
ZP252: 100 periods of 5nm/1.0nm ZnS/CdS on (100) GaAs with ZnS buffer.

C. EXPERIMENTAL TECHNIQUES

PL spectra were excited using an Ar^+ laser or ion laser/dye laser combination for wavelength selection and with ND filters (Ealing) to vary excitation densities within the range $10mW/cm^2$ to $1kW/cm^2$. Samples were maintained at constant temperature (between 10 and 300K) in a Leybold cryorefrigerator equipped with optical access via quartz windows. Sample fluorescence was

dispersed in a 1m grating monochromator with 500nm blaze and detected by photomultiplier tube or Ge photodetector. Signals were conditioned and recorded on disc using a Stanford Instruments data acquisition package. For excitation spectroscopy the detection monochromator is set at the peak of the luminescence band and the wavelength of the exciting radiation varied. The variation in emission intensity is then recorded as a function of the excitation wavelength, after correcting for constant excitation intensity.

PL decays were measured in a time domain fluorimeter, which uses nitrogen spark gap excitation at 337nm and conventional time-correlated single photon counting electronics to build up a histogram of delay times for *individual* fluorescence events. This technique measures the duration of events which begin with the generation of an electron-hole pair and end with the radiative recombination of the minority carrier in a selected radiation channel. The 337nm radiation may penetrate to the buffer or substrate layer and excite both buffer and superlattice. The emitted light is dispersed in a 0.125m monochromator equipped with a 500nm blazed grating. The minimum wavelength resolution is 2nm. Time-resolved spectra are produced by electronically setting a data acquisition window and repetitively scanning the detection wavelength. The spark repetition rate is kept low (~10kHz) to avoid aliasing and typical run times are of order 5×10^4s.

It is possible to recover the homogeneous width from the inhomogeneously broadened profile. The underlying nature of the technique is shown in Fig. 2. An inhomogeneously broadened optical transition of full-width at half-maximum, Γ, is probed by a narrow laser line of width $\Gamma_\ell < \Gamma_h << \Gamma_{inh}$. Electronic centres whose transitiona energies are within Γ_h of the laser wavelength λ_ℓ absorb this radiation, and then emit a single homogeneously broadened line at wavelength λ_ℓ with half-width $\Gamma_h = \tau_R^{-1}$, where τ_R is the lifetime of the emitting state. This is termed *fluorescence line narrowing* (FLN). When the laser beam is intense that homogeneously broadened component of the absorption band resonant with the laser line may be saturated, so that it no longer contributes to the absorption profile. The phenomenon of the reduced absorption of the saturated homogeneous component at wavelength λ_ℓ is referred to as *optical hole burning* (OHB, Fig. 2). Strong electron-phonon coupling produces homogeneously broadened absorption and emission bands (Γ_h ~ 1000cm^{-1}): neither FLN or OHB are then effective in reducing the width of optical spectra. Exciton lines in semiconductor MQWS and SLS are not vibronically broadened and in general $\Gamma >> \Gamma_h$.

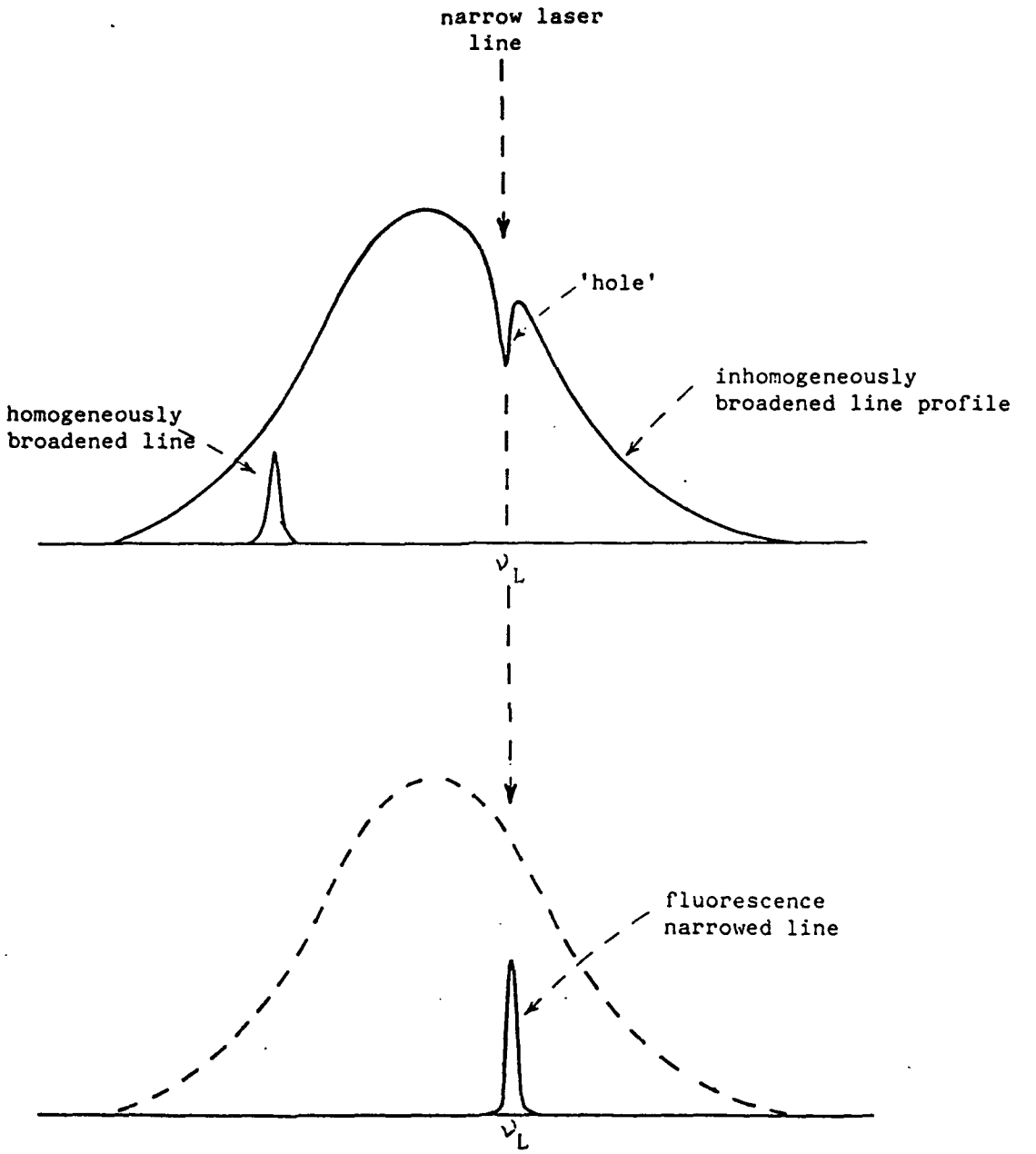

Figure 2 Optical hole burning and fluorescence line narrowing of an inhomogeneously broadened spectroscopic line.

Circular polarization measurements were made in magnetic fields up to 4.0T, using a superconducting magnet with optical access in conjunction with a photoelastic modulator operating at 27kHz plus quarter waveplate to analyse the circularly polarized emission. Essentially the modulator enables σ_+ and σ_- polarized light to be selected before measurement by the photodetector. By use of phase-sensitive electronics at 27kHz the output from the lock-in amplifier is proportional to the magnetization of the sample

$$\text{i.e. MCP} = \frac{\sigma_+(\lambda)-\sigma_-(\lambda)}{\sigma_+(\lambda)+\sigma_-(\lambda)} = -\frac{1}{2}\tanh\left[\frac{g\mu_B B}{2kT}\right] \qquad (3)$$

showing that the MCP signal is wavelength (λ), magnetic field (B) and temperature (T) dependent. Spin polarization results from quantization of the electron magnetic moment along the magnetic field, and is determined by the difference in occupancy of the $M_s = \pm\frac{1}{2}$ levels. Since these levels emit different senses of circularly polarized light the spin polarisation may be measured optically (1). Indeed

$$\text{MCP} = \frac{\Delta I}{I} = -\frac{1}{2}\tanh\left[\frac{g\mu_B B}{2kt}\right] \qquad (4)$$

If we now apply microwaves at the resonance frequency $\nu = g\mu_B B/h$, we may equalize the populations of the $M_s = \pm\frac{1}{2}$ levels and so destroy the circular polarization (i.e. $\Delta I \to 0$). The experimental arrangement of the ODMR spectrometer operates at both ν = 9.5GHz and ν = 35GHz. Assuming g=2.00 the resonance for free electron spins occurs at ca B=0.34T and B=1.25 respectively. The experiment operates at fixed frequency and the static magnetic field is scanned from 0 - 5.5T, while measuring this value of $\Delta I/I$. At resonance $\Delta I/I$ becomes zero, thereby signifying that the resonance condition is satisfied. The sensitivity of this technique relative to ordinary ESR is in the ratio $(\nu opt/\nu micr) \approx 10^4$. Once an ODMR spectrum has been recorded the field may be fixed at resonance and the dependence of the ODMR or absorption/emission wavelength recorded via the scan control of the monochromators. A recent modification to the ODMR spectrometer provides for far-infrared (FIR) laser excitation of the sample in place of the microwave radiation. This additional sophistication provides for the observation of *optically detected cyclotron resonance (ODCR)* in the two-dimensional electron gas [9].

D. EXPERIMENTAL RESULTS

(i) Donor-Acceptor Recombination in Zn-doped AlGaAs Epilayers.

The luminescence strongly reflects the composition variable, x, which as Table 1 shows varies from 0 to 0.5. In each case the emission takes the form of a broad unstructured band the peak wavelength varying from 835nm with x=0 to 602nm for x=0.50. However, the wavelength shift, linear in x between x=0 and x=0.23 changes slope at this composition when the material changes from direct gap to indirect gap, Figure 3. In all cases the decay processes are multi-exponential, as is characteristic of D-A recombination for which the peak energy is given by

$$h\nu = \Delta_G - (E_D + E_A) + \frac{e^2}{4\pi\epsilon_o Rij} \qquad (5)$$

Obviously the smaller Rij, the D-A separation, the shorter the wavelength and radiative lifetime of the D-A emission. The effect of this type of inhomogeneous broadening is evident in Figure 4 which shows the luminescence decay profile of the $Al_{0.3}Ga_{0.7}As$ sample at λ=610nm, 632nm and 657nm. Obviously $\tau_R(610 < \tau_R(632) < \tau_R(657)$ although none of the decay curves is a single exponential.

(ii) Quantum Confinement in MQWs and SLSs

Figure 5a shows the steady state photoluminescence spectrum for a GaAs/AlGaAs MQW (Sample KLB219) measured at T=10K. At such a low temperature, recombination involves only the lowest energy states in the conduction and valence band wells i.e. the n=1 electron state and n=1 heavy hole state. We refer to the E_{hh}^1 luminescence, which occurs at a wavelength of 783.5nm. This corresponds to an energy of 1.583eV, greater than the band gap energy of GaAs, demonstrating clearly the effect of quantum confinement. The excitation spectrum of this emission is shown in Fig. 5b. Clearly evident are the 1e↔3hh, 2e↔2ℓh and 2e↔2hh transitions. Similar behaviour is observed for sample KLB155, albeit at rather shorter wavelengths on account of the narrower well structure. Using well widths varying from 2.0nm to 30nm gave the results shown in Figure 6, a plot of log E, versus log L_z, E being the emission peak energy. There is a linear decrease in E with L_z with slope -1.71: it is recalled that the infinite potential well model leads to shifts varying with L_z^{-2} from the position of the bulk exciton at 1.41eV.

II-VI compound SLS show similar effects due to quantum confinement. In a single, thick ZnSe epilayer the emission occurs at 443.5nm. By comparison, a

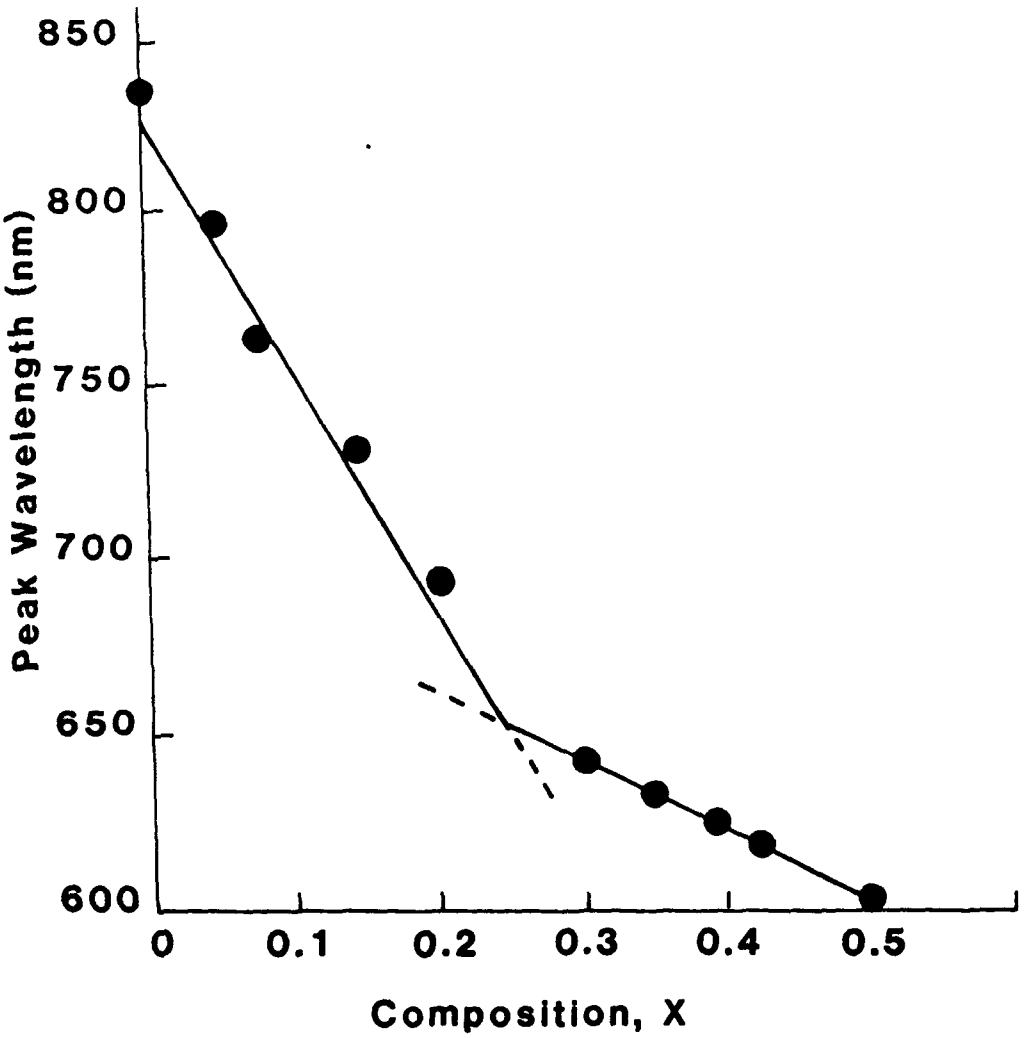

Figure 3 Wavelength shift with composition, x, of D-A recombination luminescence for Zn-doped $Al_xGa_{1-x}A_1$.

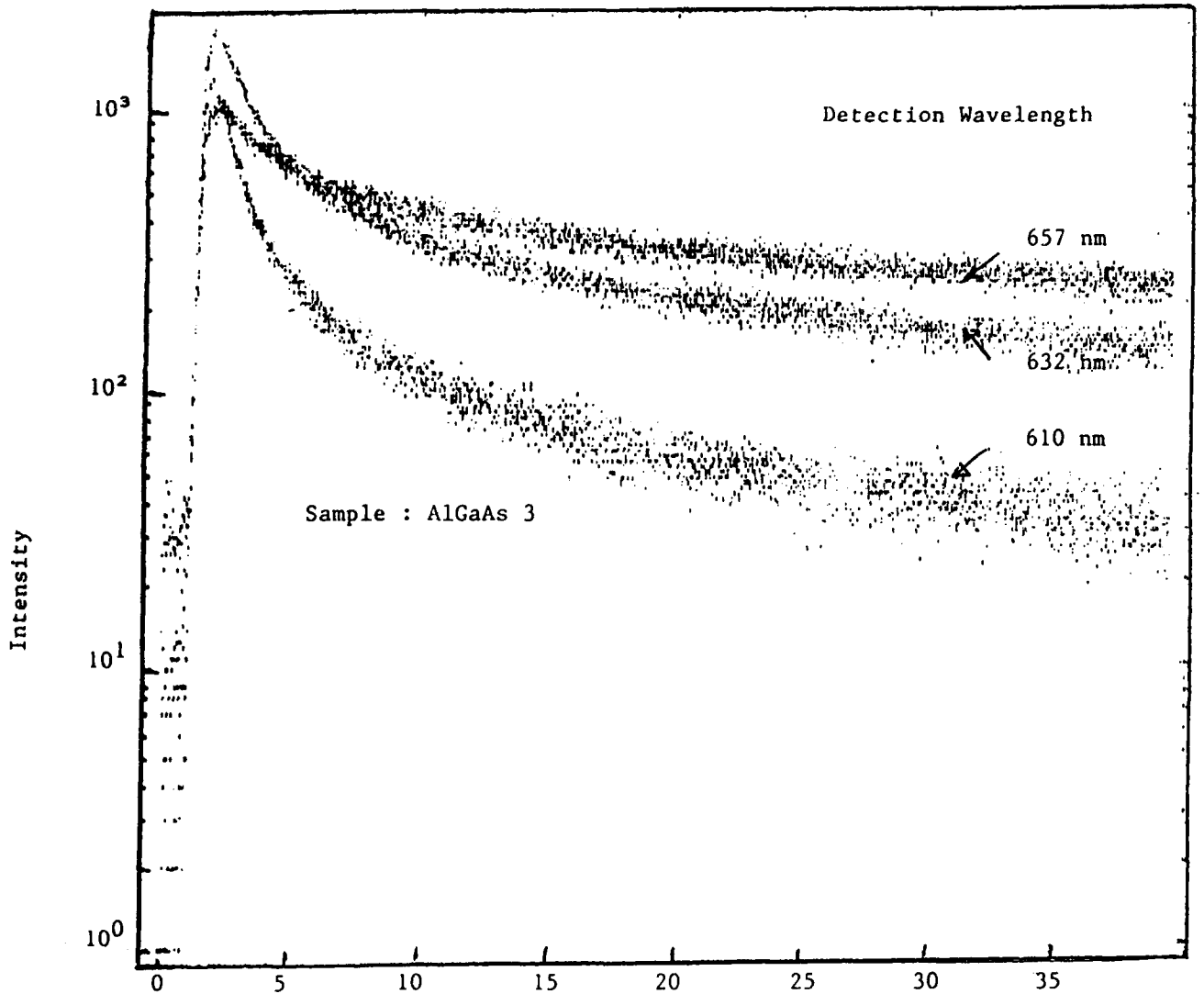

Figure 4

Showing the effects of inhomogeneous linebroadening on D → A recombination in Zn:AlGaAs epilayer samples at 77k

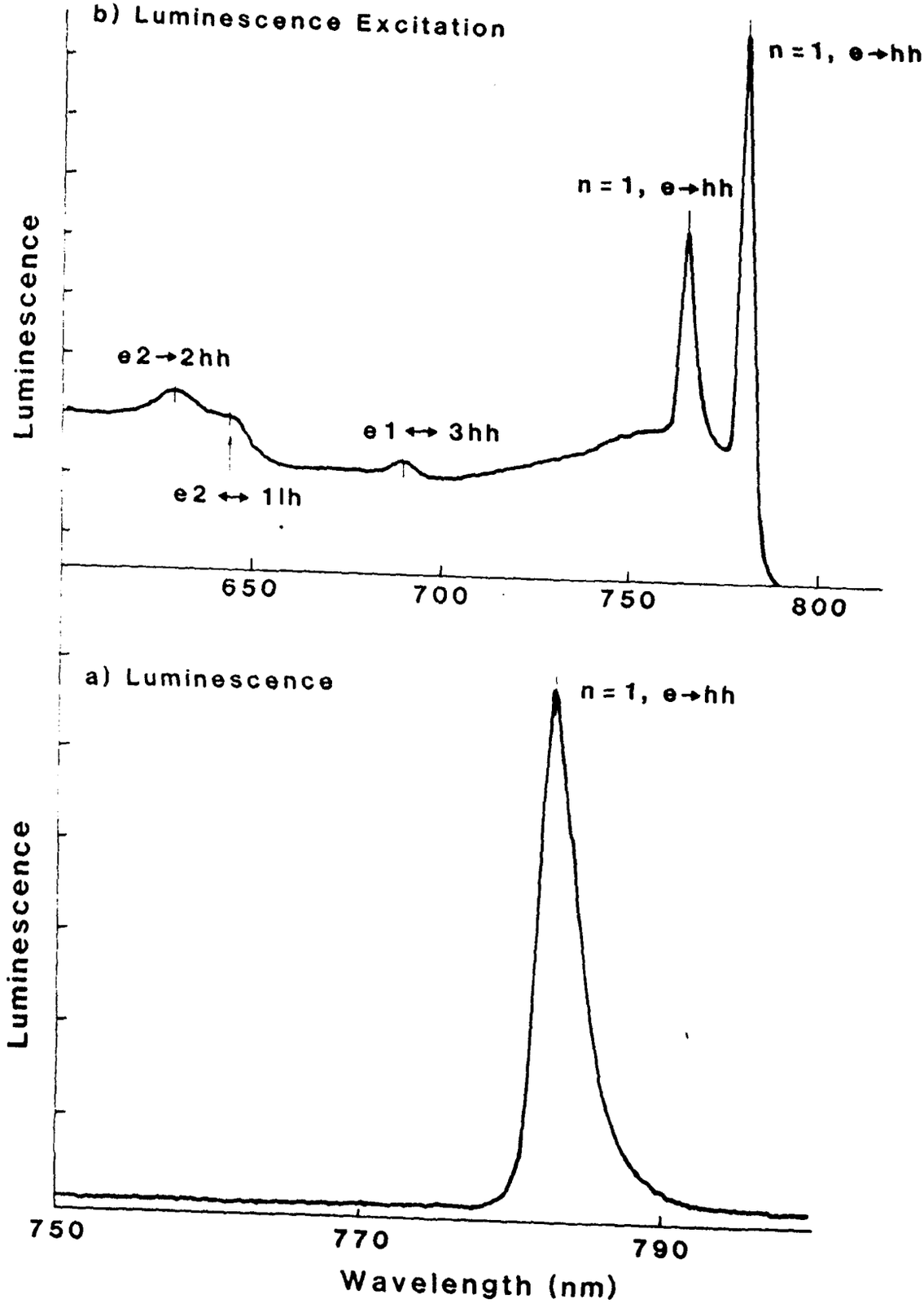

Figure 5 PL and PLE spectra of a MQWS consisting of 15 GaAs layers of thickness L_z = 6.5nm and barriers of width 175nm measured at 10K.

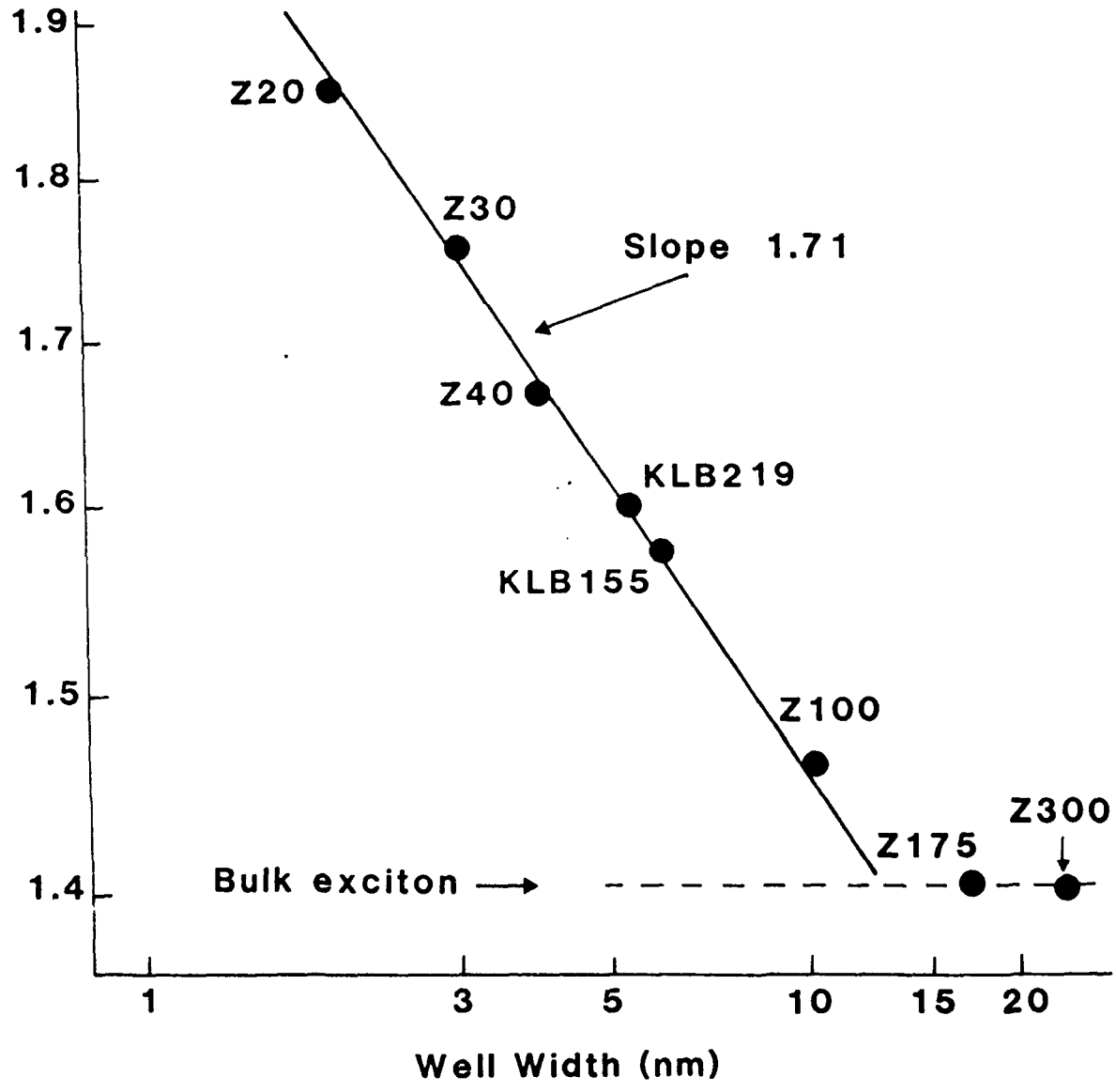

Figure 6 The PL peak energy plotted as a function of well width, L_z, on a log-log format. Samples KLB courtesy Philips Research Labs and samples Zn courtesy Dr J. Zavada.

SLS comprisisng 100 periods of 0.6nm thick ZnSe wells with 5.4nm thick ZnS barriers which emits at 406nm. As shown in Fig. 6 for GaAs/AlGaAs quantum wells a log-log plot of λ versus L_z for ZnS/ZnSe SLS with different well widths is linear, the slope in this case being -1.77. A comparison of the behaviour of ZnS/ZnSe, ZnSe/CdSe and CdS/CdSe superlattices is shown in Fig. 7. Both ZnS/ZnSe and ZnSe/CdSe are examples of Type I superlattices (Fig. 1), the emission peak being shifted to higher energies relative to bulk ZnSe and CdSe respectively.

Fig. 7 shows that the steady state photoluminescence of hexagonal CdS/CdSe SLS is dominated by a strong broad emission band below the CdSe (wurtzite) fundamental absorption edge. Emission from superlattices with longer periods is shifted to still longer wavelengths. For example, in a superlattice with equal well and barrier widths of 1.3nm, the luminescence peak is at 740nm, whereas with wells and barriers of equal width 5.4nm, the peak is at 950nm. This behaviour is interpreted as recombination between quantum confined electrons and holes in a type II superlattice, Figure 8. Electrons confined in the 0.25eV conduction band quantum well (in CdS) recombine with holes trapped in the deeper CdSe valence band well. The flat bands show the situation in the absence of piezoelectric fields. The piezoelectric field "tilts" the bands in opposite senses in adjacent layers. The potential drop across a period is zero, since there can be no sustained potential difference between the top and bottom of the sample. With the piezoelectric fields of order 0.1 volt per nanometre wider layers support larger potential drops [10]. Hence structures with longer periods have smaller effective bandgaps and emit at longer wavelengths.

(iii) Exciton Luminescence Lineshapes

A comparison of the luminescence and excitation spectra for samples KLB219 (Fig. 5) and KLB155 show energy shifts between the E_{1h} emission and excitation peaks of <0.5meV for KLB219 and 2meV for KLB155 (Fig. 9). The luminescence linewidth is very much larger than that in bulk GaAs. The shifts are strain-induced. This was shown by measuring the emission from both a 'free-standing' KLB219 sample and a sample under strain applied by coating the rear of the sample with aquadag prior to cooling to cryogenic temperatures. Strain-induced shifts greater than 4MeV were observed. However, KLB155 showed higher energy structure due to the $E_{1\ell}$ emission, giving rise to a far greater sensitivity of the band width to increasing temperature. In these GaAs-AlGaAs superlattices we have not observed fluorescence line narrowing during resonant excitation: lifetimes of order 200-300ps preclude resolution

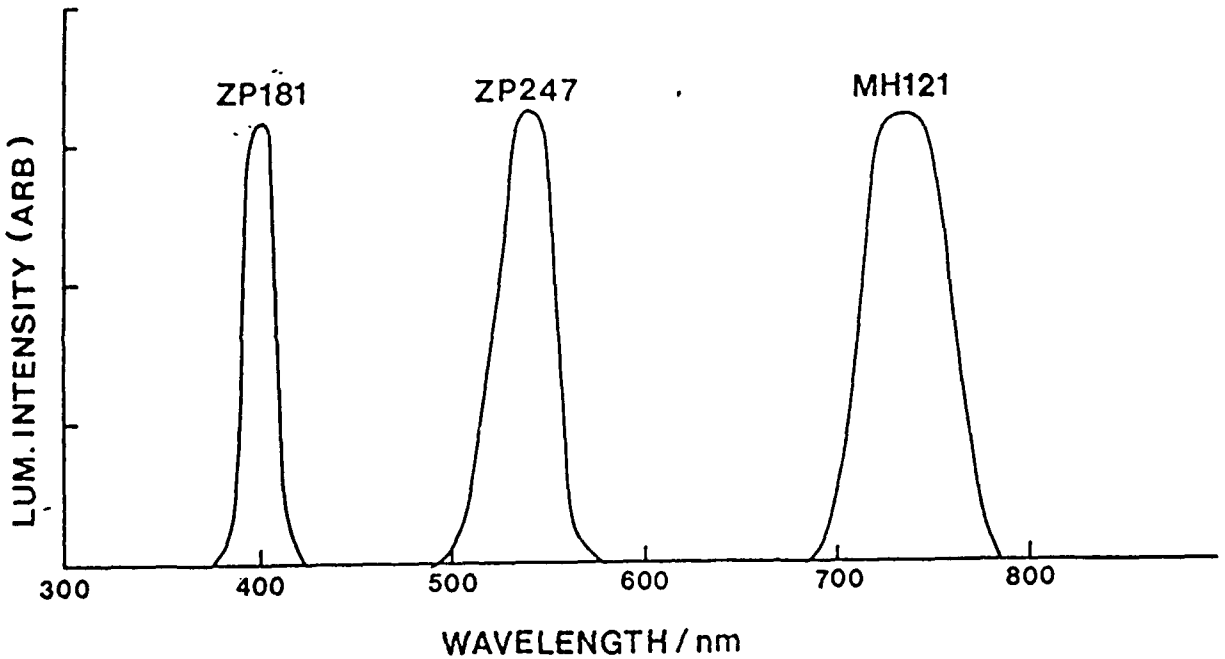

Figure 7. Typical exciton photoluminescence from II-VI compound strained layer superlattices measured at 90K.

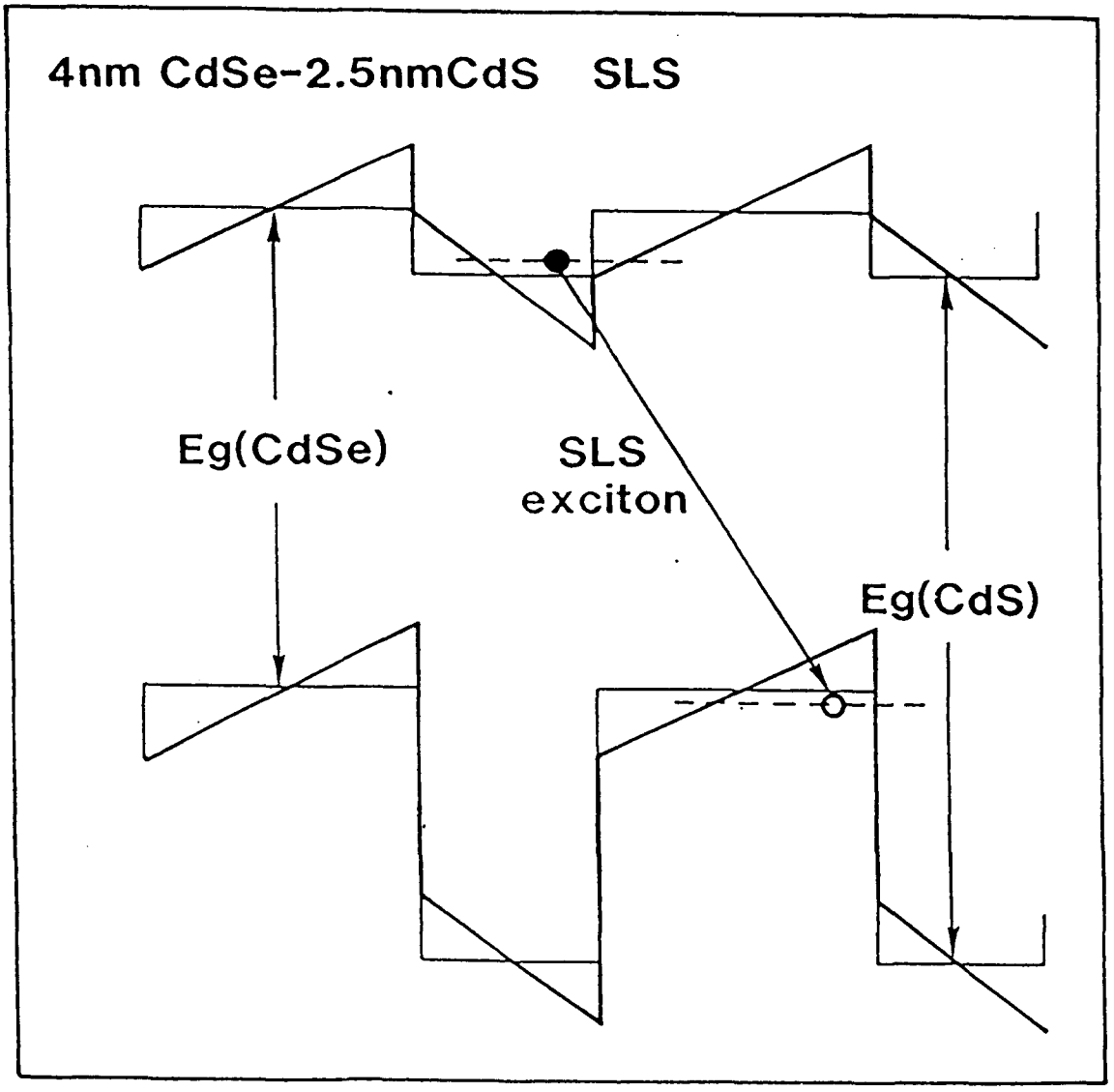

Figure 8. Band structure of a typical type II-superlattice, with and without piezoelectric fields. The superlattice exciton recombination process is indicated.

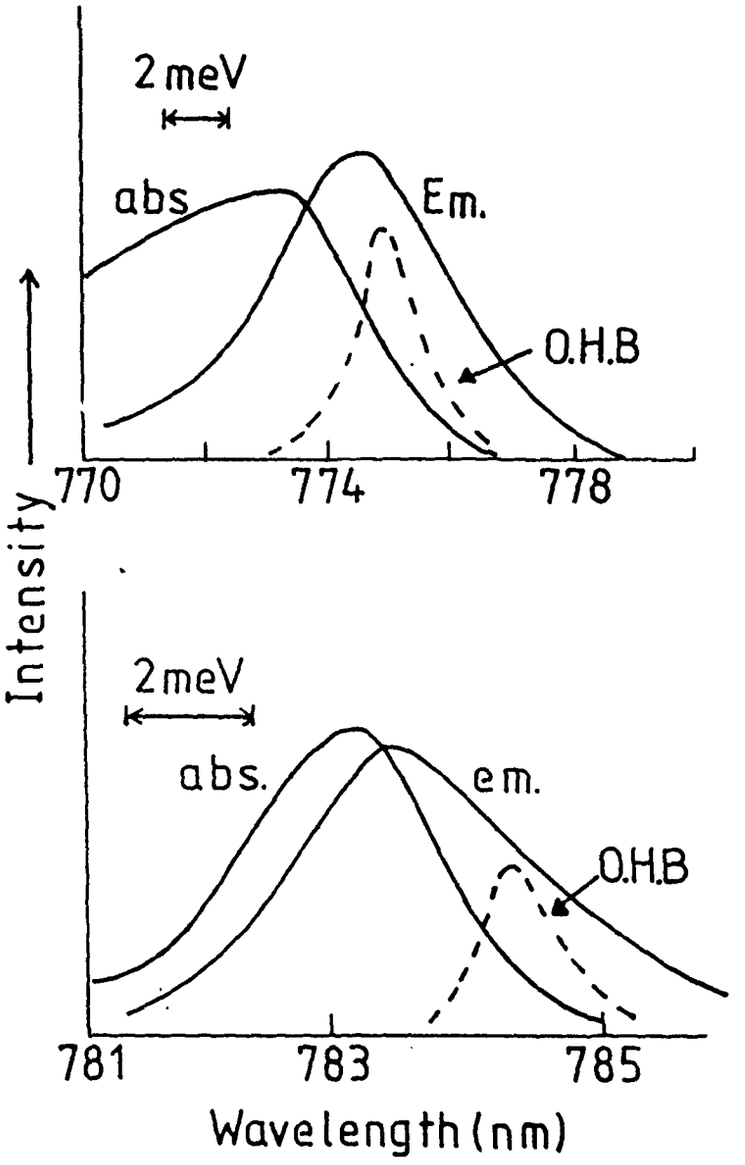

Figure 9. Shape of 1e - hh transition in (a) samples KLB155 and (b) KLB219 measured in absorption (abs) and emission (em). The homogeneous profile is shown by the optical hole-burning line (OHB).

with the present detection system. The homogeneous width estimated from measuring the propagation delay of a single pulse used to burn a hole in the absorption profile is shown schematically in Fig. 9. In these measurements Γ_h varies across the absorption profile: the results being ca 0.5meV in the long-wavelength of the exciton line and greater than 1meV above the peak. Such results imply localisation at energies below the band peak [11].

A rather novel behaviour is observed for the piezo-electric ZnSe/CdSe SLS. As Figure 10a shows the overall exciton bandshape for MH95 is gaussian, being a convolution of contributions from wells with widths of one lattice spacing up to ten, the mean width being 5 spacings. The sequence of selectively excited luminescence 10b - f show the effects of fluorescence line narrowing. Clearly observed are the resonant line and its phonon replicas from excitons localised by disorder as well as the broad resonance due to delocalised excitons. The resonant line is too narrow to be measured using the 1m grating monochromator, which has a resolution of 0.02nm. By making use of the polarisation properties of the FLN it is possible to resolve six orders in the phonon assisted sideband. That the separation between the phonon peaks varies with excitation energy is thought to be due to alloy disorder. A plot of the modulation depth I_b/I_o with excitation wavelength is linear reaching a maximum value of unity near λ = 530nm. This wavelength essentially marks the mobility edge. These results are both novel and preliminary and these II-VI compounds are the subject of further work.

(iv) Non-linear Optical Effects

For both KLB155 and KLB219 samples excitation spectra obtained by monitoring the luminescence at the peak of the E_{1h} emission at T=6K, Fig. 11, shows that excitation on the low energy tail of the line results in the greater part of the emission being emitted at a higher energy than that of the exciting light. In the example shown emission excited using light at 785.1nm (1.5795eV) is observed with peak at 1.5835 and a discernible tail extending to 1.5875eV. Hence the input light is being up-converted at T=6K by up to 8meV or 10kT. The up-conversion efficiency is not enhanced by temperature in the range 16-85K. This latter observation suggests that up-conversion is not induced by normal phonon-assisted processes. Rather does up-conversion involve the recombining excitons being in contact with low-lying excitations induced by well-width disorder.

Non-linear changes in fluorescence spectrum were also observed in II-VI SLSs. For a continuously excited CdS/CdSe sample, the exciton luminescence peak

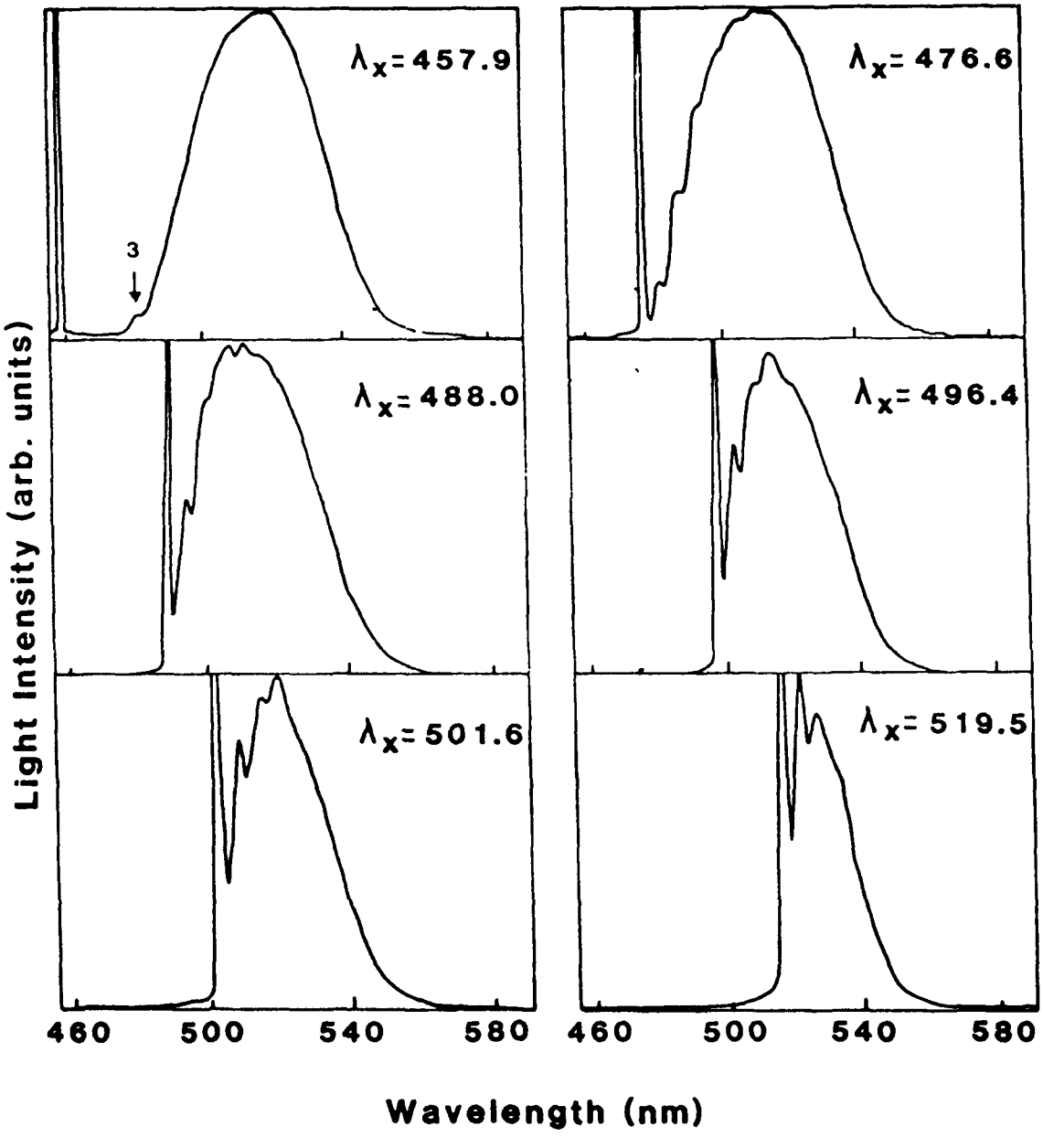

Figure 10 FLN spectra for a ZnS/CdSe superlattice

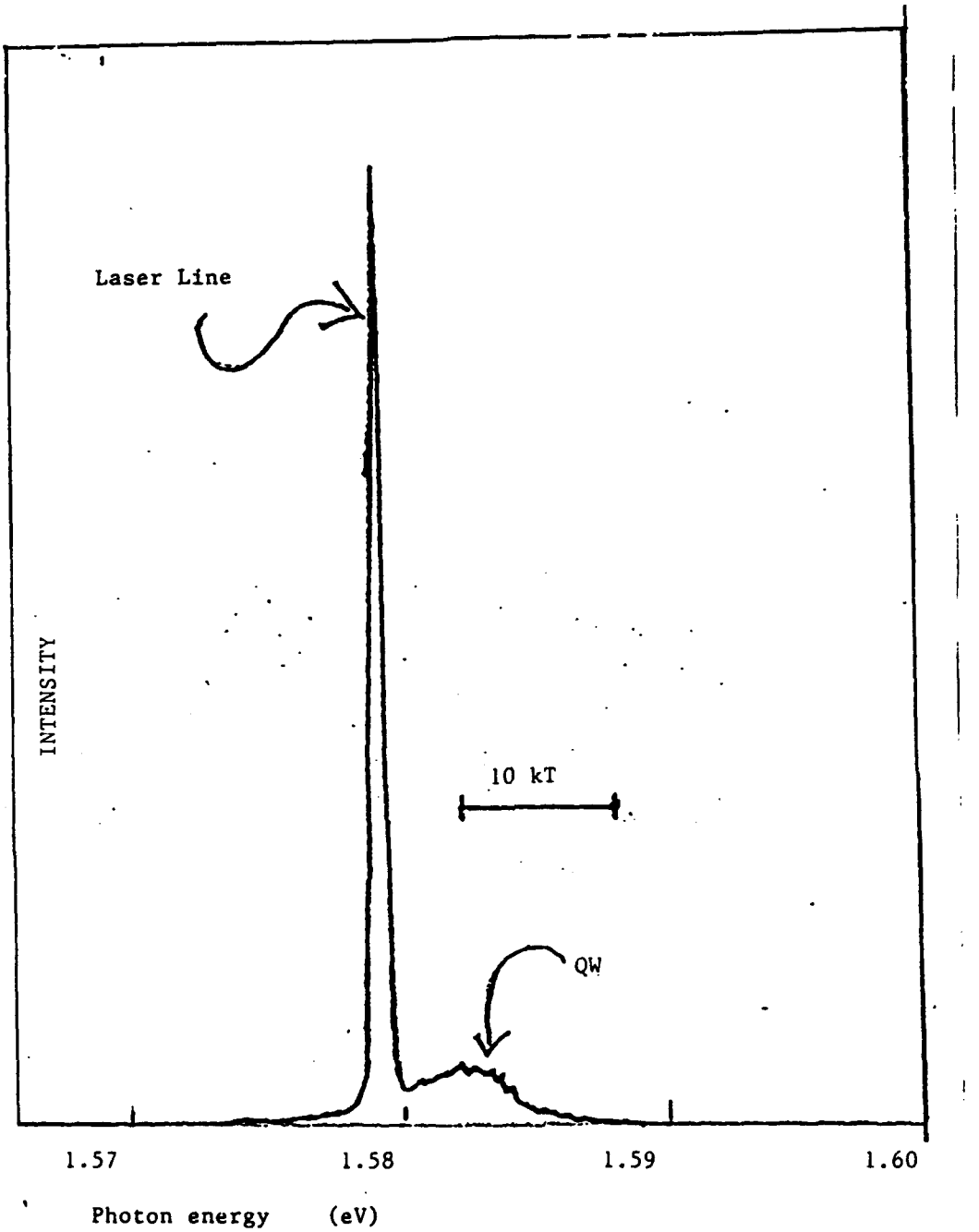

Figure 11

Showing up conversion of laser light in GaAs/AlGaAs QWs (Sample KLB.155)

depends on the excitation power density in several important ways. While the total integrated intensity increases linearly, the peak shifts to higher energy and narrows as the excitation power increases. The onset of photoexcitation results in a build-up of carriers which drift to the superlattice interfaces under the influence of the internal fields. The electrons and holes, separately trapped in CdS and CdSe layers, respectively, then screen the piezoelectric fields. The equilibrium populations of the separated charge carriers depend on the carrier generation rate which in turn depends on the excitation power density. In consequence, the degree of screening determines the nett electrostatic potential drop across each layer, so that the effective bandgap depends on the incident light intensity.

(v) Luminescence Decay and Time-resolved Spectroscopy.

Measurements of luminescence decay for the GaAs/AlGaAs MQWS revealed that for both KLB155 and KLB219 samples the excited state lifetime is quite short: however, the decay is not singly-exponential. However, depending upon the state of strain the initial decaytime is between 500-800ps, this representing the fluorescent lifetime of the singlet exciton [11]. Nevertheless, the longer term decay ($t \sim 10^{-6}$s) is non-exponential, a characteristic related to dispersive relaxation. This rapid relaxation is typical of the behaviour of type I superlattices, where there is no spatial separation of the differently charged carriers. Similar measurements have also been made on an AlAs/GaAs type II superlattice in which the exciton luminescence peak occurs at 790nm. The electron and holes are localised in the conduction band of GaAs and valence band of AlAs, respectively so that the timescale of the decay is longer. The decay over four decades of time (to 10^{-2}s) fits the stretched exponential [12]

$$I(t) = I(o) \exp\left(-t/\tau_R\right)^{\beta}$$

where $\tau_R \simeq 10^{\pm 3}$ns and $\beta = 0.48 \pm 0.5$. A more detailed study has been made of the decay characteristics of the piezoelectric CdS/CdSe superlattices. Sample MH95 is a relatively thick superlattice consisting of 20 periods with CdS and CdSe layers of 2.5nm and 4nm, respectively, grown on a CdS buffer layer to minimise the mismatch with the (111)A GaAs substrate. The time-integrated photoluminescence spectrum (from zero delay to 10μs) of this sample measured at 10K is shown in Figure 12. The main peak near 740nm in Figure 12, is the superlattice exciton, occuring at energies below the band edge at 1.83eV. The deconvoluted peak at 677nm is due to a direct recombination of electrons and holes within the CdSe layers. It decays

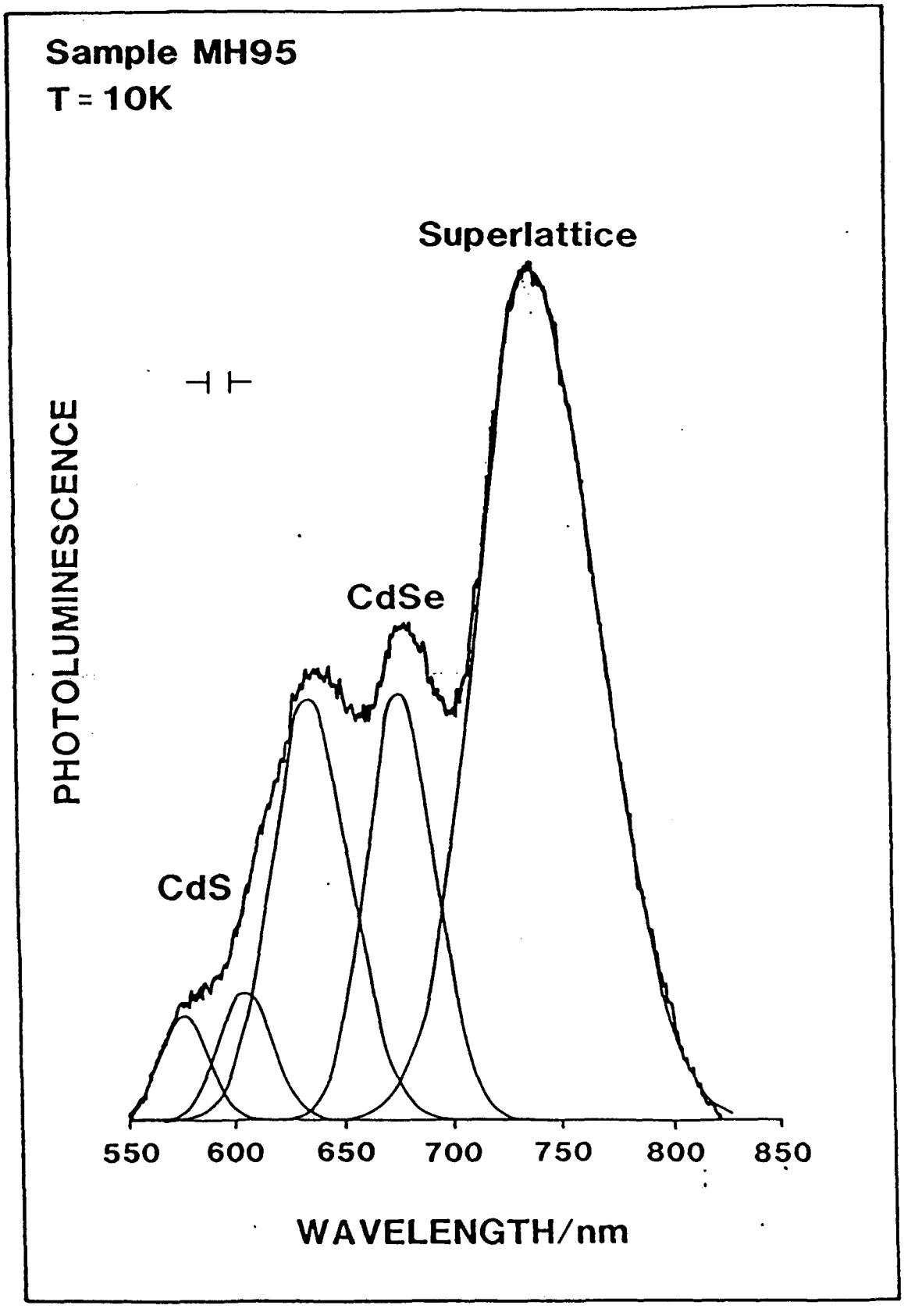

Figure 12 Time-integrated PL spectrum of a typical CdS-CdSe superlattice.

within a few nanoseconds, as is expected for a direct transition in CdSe, albeit one broadened by the effects of random lattice strain and electric field. The three higher energy peaks are associated with deep recombination centres in the CdS buffer layer where the bandgap is 2.56eV at 10K. In time-resolved spectra, obtained with a constant time window of 60ns, Figure 13, the exciton peak broadens and shifts to longer wavelengths as the initial delay increases from zero to 2μs. The variations are rapid after short delays, but tail off at longer delays. The total peak shift amounts to about 5% of the band gap. Although photoluminescence decay is normally used to measure carrier lifetimes directly, it is no straightforward matter to monitor the luminescence decay of a band shifting to longer wavelengths in time. When the decay is monitored at fixed wavelengths in the exciton peak the initial decay rate decreases as the wavelength increases. The decay curves are markedly non-exponential. The example in Figure 14 shows the decay profile obtained using a 750nm interference filter with 80nm bandwidth to integrate the emission over the whole exciton band.

vi) Magnetic Circular Polarization and Optically Detected Magnetic Resonance

Measurements have so far been made for sample KLB155. The sample was illuminated with some 10mW/cm^2 of the He-Ne laser radiation and light detected in the Faraday configuration. The spectra were excited using unpolarized, σ_+- and σ_--polarised radiation at 1.6K, 4K and 10K. Typical data, given in Figure 15 show that the emitted light is strongly polarized in a magnetic field, that the polarization increases with magnetic field but decreases rapidly with rising temperature. The magnitude of the CPE signal is also strongly dependent upon the sense of polarization of the exciting light.

We have attempted to make ODMR measurements on KLB155 and KLB219 at both 9.5GHz and 35GHz, with microwave power levels of 50mW up to 3W in the temperature range 1.6-4.2K, so far without success. This despite the fact that the emitted radiation is strongly circularly polarized, usually an indicator of strong ESR. It is evident that there is insufficient microwave power. The key to this is the radiative lifetime of the emission, a quantity that we have measured. The decay process is not a single exponential decay, there is a very fast process $\tau_R \approx 10^{-11}$s and a rather slow process $\tau_R \approx 3\times10^{-8}$s: most of emission decays via the fast process. To reduce $\Delta I/I$ to zero via microwave pumping requires sufficient microwave power to saturate the ESR transition in the time available before recombination occurs. This required that $g^2\mu_B^2B_1^2T_2 > \tau_R^{-1}$, where B_1 is the microwave magnetic field at the specimen and T_2 is the spin-spin relaxation. For microwave cavities and

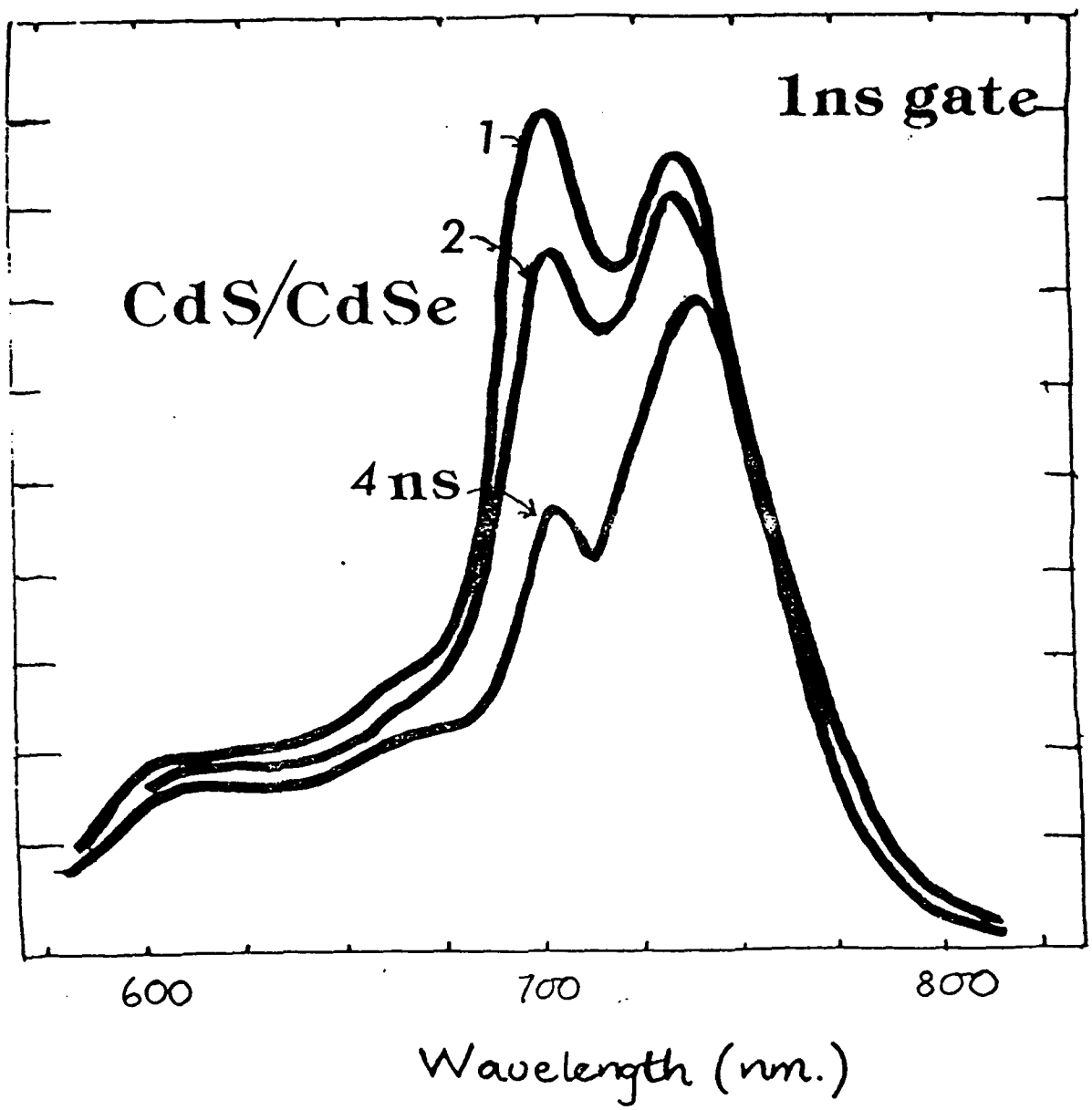

Figure 13 Time-resolved photoluminescence, on a nanosecond timescale, of the intrinsic Stark superlattice CdS-CdSe. Spectra at 1ns, 2ns and 4ns delays show the relatively fast decay of the CdSe real-space-direct exciton near 700nm. The superlattice exciton, near 740nm, is relatively long-lived; it broadens and shifts at longer delays due to the intrinsic Stark effect.

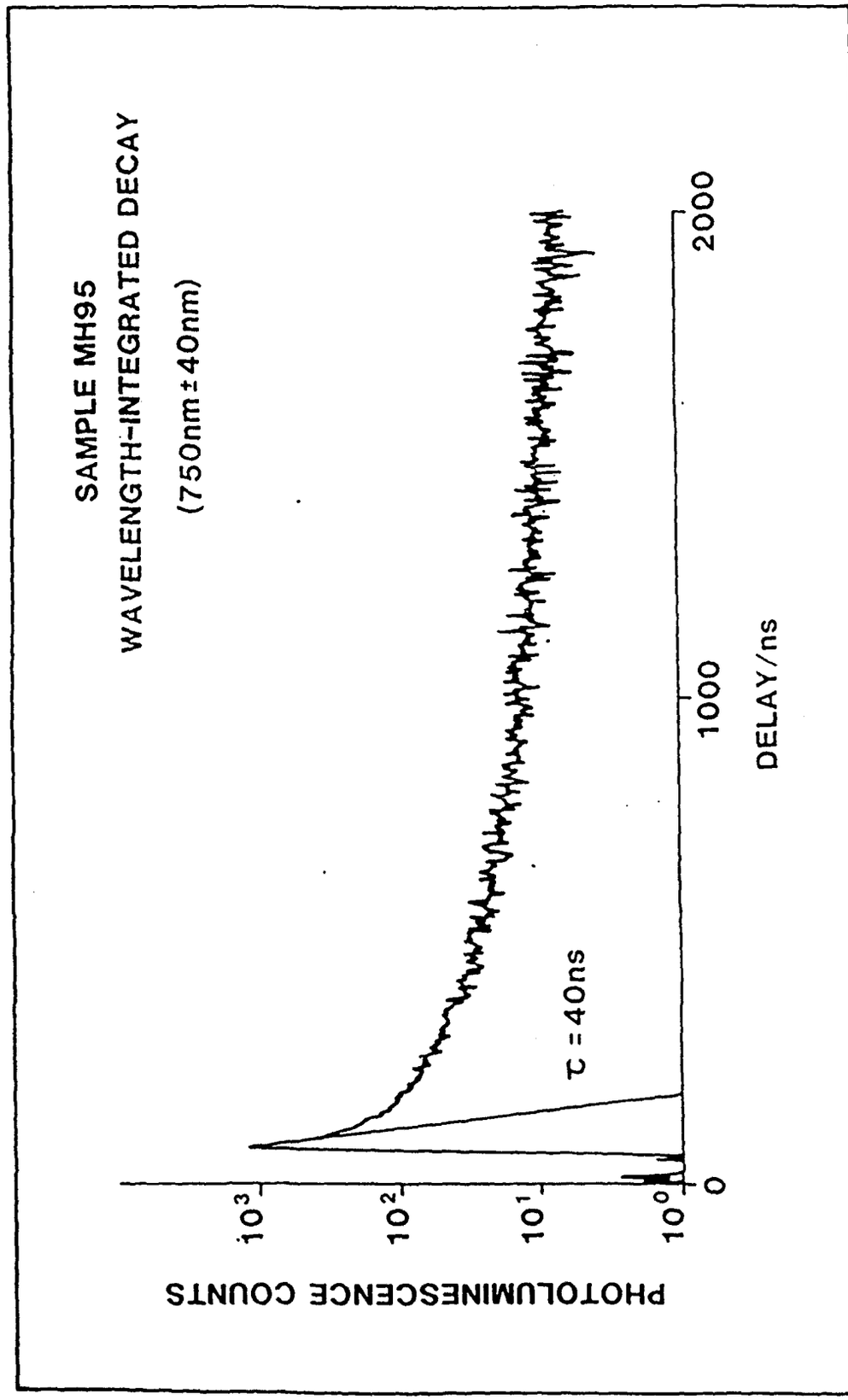

Figure 14 Decay profile of the exciton emission in CdS-CdSe superlattice MH95

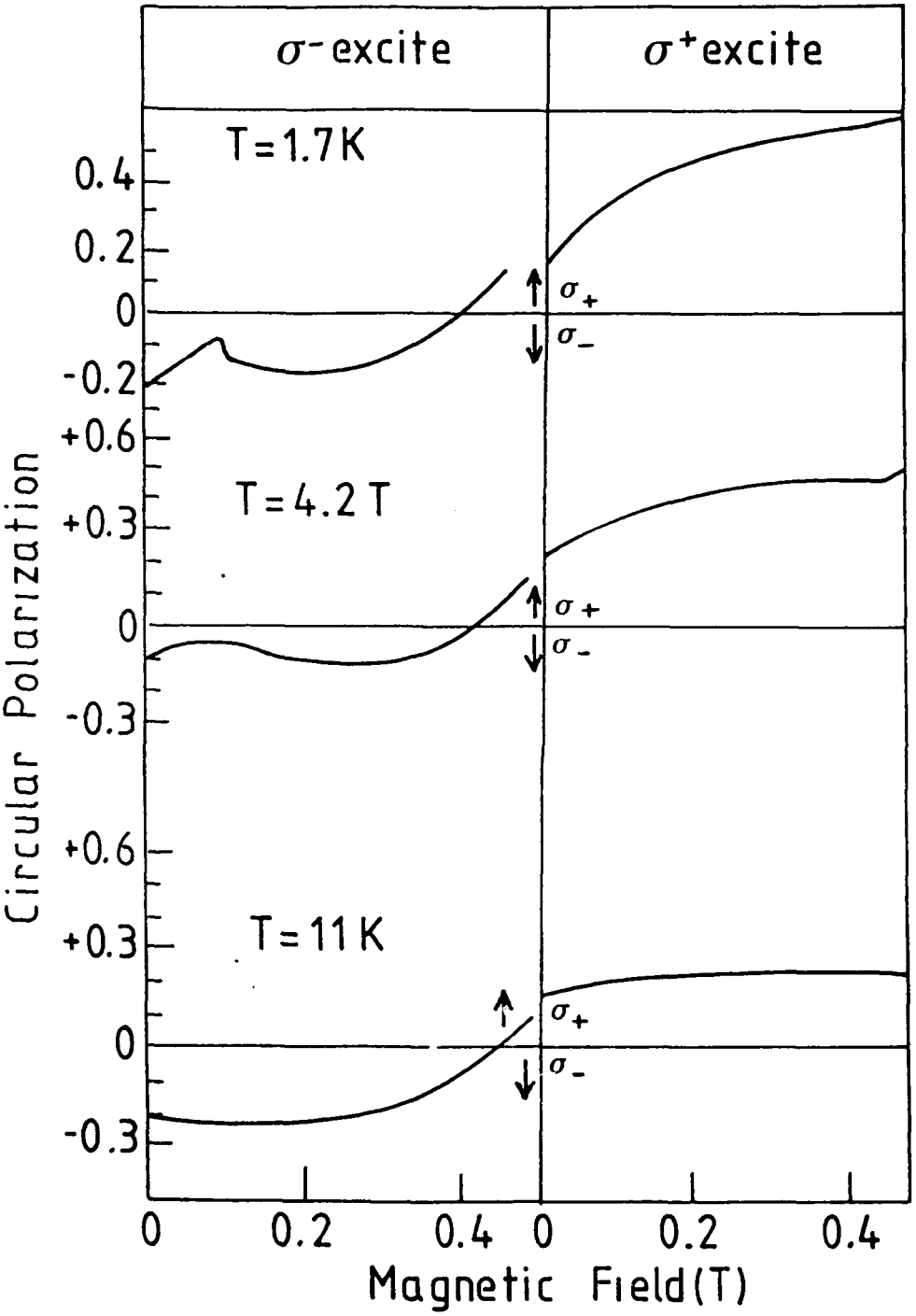

Figure 15 Circularly polarized emission from GaAs/AlGaAs MQW (KLB219).

power levels in excess 1W as used in ODMR $B_1 \sim 10^{-3}$ and T_2 is around 10^{-6}s. It therefore becomes difficult to cause appreciable changes in ΔI if $\tau_R < 10^{-8}$s. Thus for rapidly recombining systems very high microwave power is required but then one encounters lifetime broadening of the resonance signals. A lifetime of 10^{-9}s produces a broadening of order 10^{-8}eV, corresponding to a linewidth of 15mT at g=2.0.

Although we have not identified the ODMR spectrum of recombining carriers in MQWs KLB155 and KLB219, we have observed ODCR in GU154. Figure 16a shows the photoluminescence spectrum of this sample measured at 4.2K. Clearly identified is the single emission peak for each well thickness due to the lowest energy free exciton in each well. Note the decrease in the FWHM of each emission line with increasing value of L_z. These exciton lines are clearly identified in the spectral dependence (Fig. 16b) of ODCR induced by FIR laser radiation at λ=163μm in a magnetic field of B_o=4.8T. This is just the field at which cyclotron resonance leads to a decrease in the luminescence emissions for the 17.0nm well, Fig. 16c. An identical result obtains from the 11.0nm well. The details of these spectral features are being further investigated as are the ODCR studies of the (D^o,X) and (D^o,A^o) spectra also evident in Fig. 16a.

E. DISCUSSION OF EXPERIMENTAL RESULTS

This report is concerned with photoluminescence phenomena in a range of different epi-layer materials. In experiments on single epitaxial layers of Zn:$Ga_{1-x}Al_xAs$ the transition from direct to indirect gap is clearly observed. Exciton recombination has been studied in both III-V QWS and II-VI SLS. In these studies the position of the n=1, electron-heavy hole luminescence peak demonstrates the consequence of quantum confinement. The data in Fig. 6 are exactly as one would expect from optical transitions in a <u>finite</u> potential well in one-dimension. The $L_z^{-1.71}$ behaviour for GaAs/AlGaAs, Fig. 6, rather than L_z^{-2}, shows the effects of the 'soft' potential barriers through which carriers have a finite transmission coefficient. The results for this multiple single well sample GU154, Fig. 6, also fit onto this curve, Fig. 6, rather well. There is a remarkable similarity between excitons in LDS and F-centres in alkali halides [13] in this respect. In Zn(Cd)S(Se) superlattices (Fig. 7) the exponent is -1.83, presumably reflecting the greater ionicity of the II-VI compounds relative to the III-V compounds.

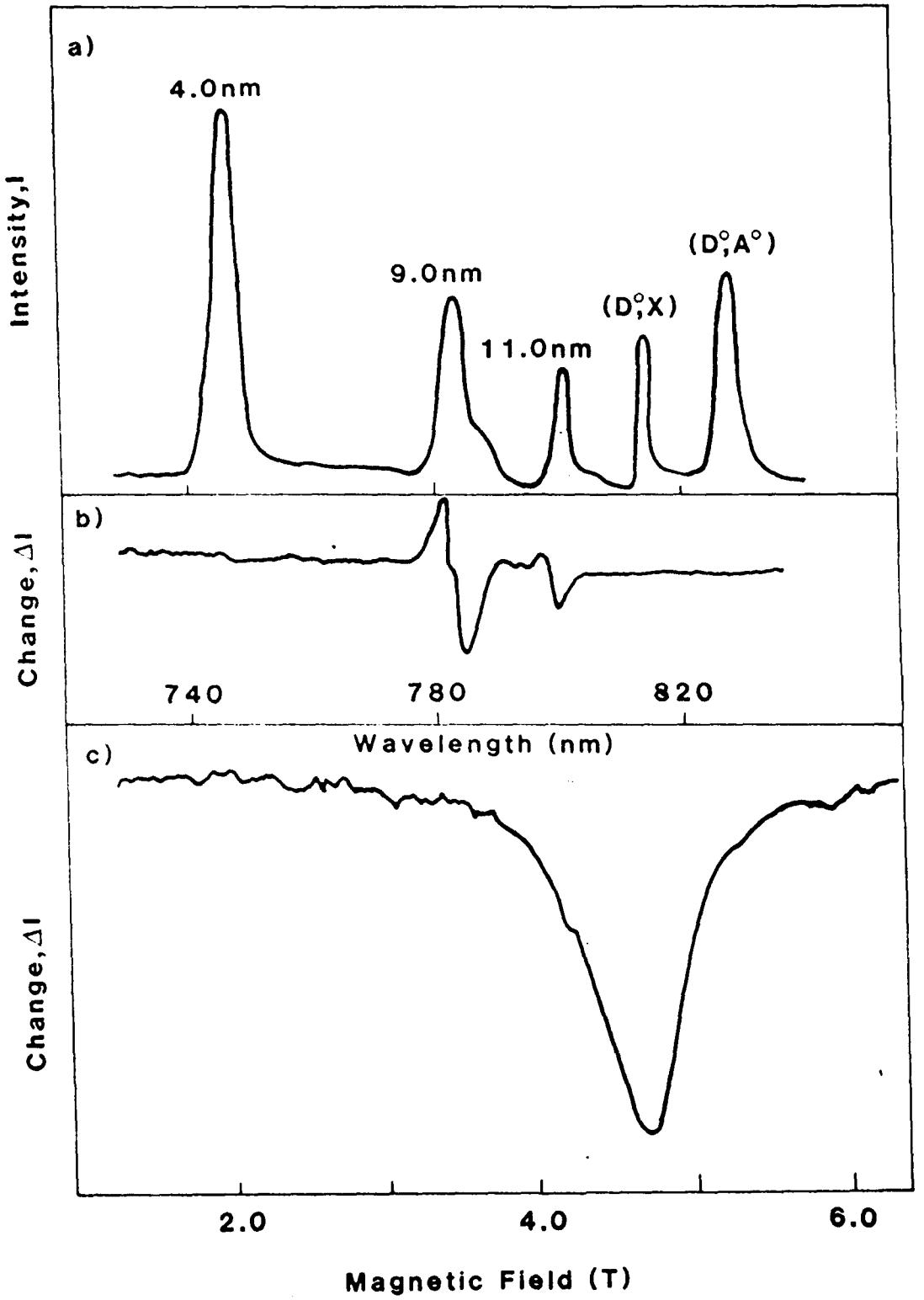

Figure 16 a) Fluorescence due to exciton luminescence in a multiple single quantum well sample, GU154, of GaAs/$Al_{0.4}Ga_{0.6}As$. There is one luminescence singal for each well width of 4.0nm, 7.0nm and 11Onm well.
b) Spectral variation in the ODCR signal detected as the change in fluorescence intensity, ΔI, induced by FIR laser radiation at 163μm in a magnetic field B=4.80T.
c) Change in fluorescence intensity from a QW with well width, L_z=7.0nm induced by FIR radiation of wavelength $\sim$-163μm as a function of magnetic field.

Photoluminescence decay processes for AlGaAs/GaAs, AlAs/GaAs and Zn(Cd)S(Se) are non-exponential (Figs. 4, 14) due to the effects of disorder. The other spectral consequence of disorder is the inhomogeneous broadening of the exciton lines (Figs. 5, 7, 9, 12). Disorder is revealed in the rather remarkable example of FLN in ZnSe/CdSe superlattices (Fig. 10) which give arguably the clearest example of an optically-detected mobility edge yet reported. The causes of disorder are several, strain, well-width fluctuations, defect structure etc. Strain has the additional consequence of inducing strong piezo-electric fields in hexagonal II-VI SLS, where the band structure diagram in Fig. 8 has particular relevance. Note that the long decay tails observed in II-VI SLS are not entirely attributable to the piezoelectric effect since they are observed in non-piezoelectric strained layer superlattices grown by MOVPE on (100) GaAs substrates [14]. The ubiquity and the general appearance of the long decay tails, e.g. Fig. 14, suggest instead that they are primarily due to the multiple sequential trapping and release of carriers at interface fluctuations. Photoexcitation by a 2ns pulse at 337nm floods the conduction and valence bands of the superlattice with excited carriers. The carriers relax to the quantum well levels and become localised near the superlattice interfaces within picoseconds. The separated carriers screen the piezoelectric fields and this drives the superlattice towards the flat band structure (Figure 8). As the electrons and holes recombine, giving rise to excitonic luminescence, the screening diminishes. The bands tilt, reducing the effective bandgap. As a result the exciton peak moves to longer wavelength as shown in Figure 13. The exciton width also increases as the field increases, as in II-VI superlattices subjected to *external* fields [14, 15]. This effect has two causes. The first is the field ionisation of the exciton which occurs when the potential drop across an exciton diameter exceeds the binding energy. The second arises from the interaction of variations in layer thickness with the field tilt, which produces a spread in the effective bandgap. The disappearance of the direct CdSe exciton band at 677nm coincides with the re-establishment of the internal fields. After a few nanoseconds, type II superlattice recombination becomes the dominant emission process, suggesting that the remaining electron population has become trapped wholly in the CdS layers. The radiative lifetime of the type-II exciton is of order 10ns, as measured from the initial decay rates shown in Figure 14. Nevertheless, many recombination events may be delayed as electrons and holes become trapped temporarily at fluctuations in the interfaces. The re-establishment of the piezoelectric fields is also slowed down by the trapping of the carriers. With increasing delay the quantum wells become deeper and electrons and holes

which remain in the bands increase their spatial separation, thereby reducing the probability of recombination [15]. The effective lifetime therefore increases with time, as is reflected by the increasing radiative lifetimes as the well width increases [16, 17]. In fact, the measured decay times are *similar* for samples with different well widths. This indicates that the trapping of carriers dominates the statistics of the emission process, even at the shortest delays. On the other hand, the peak shifts are larger in superlattices of larger period in a way entirely consistent with the piezoelectric field model, as described earlier. The measured initial decays are faster at shorter wavelengths because the emission band 'slips away from under' the detection wavelengths. The equivalent 'decay time' of about 15ns at 700nm corresponds to an optical switching time at this wavelength.

In a magnetic field the exciton luminescence in GaAs/AlGaAs quantum well samples is strongly circularly polarised as is shown inFig. 15 for sample KLB155. It was surprisisng, then, that ODMR associated with recombining electrons and holes was not detected at X-band or Q-band. Consultation with Fig. 16 suggests that this may be due to the exciton orbital radius exceeding the well width (in this case L_z=5.0nm). In Figure 16 optically detected cyclotron resonance is only detected in the well widths $L_z \geq 7.0$nm. Figure 16b shows that for both the 7.0nm and 9.0nm ODCR is evidenced by a change in luminescence intensity at a resonance field of 4.8T induced by the FIR radiation with wavelength λ=163μm. No such effect is observed for the 4.0nm well. The changes in the 7.0nm well ODCR signal correspond to an increase in intensity, ΔI, on the short wavelength side due to free exciton emission at the expense of the longer wavelength emission due to bound excitons. The field at which the ODCR signal is observed, Fig. 16c, corresponds to an effective mass of m^*=0.074 for B||[001]. Essentially the bound excitons are ionised by the FIR radiation, thereby decreasing the bound exciton luminescence intensity and supplementing the free exciton luminescence.

TABLE 1 Photoluminescence daa for $Al_xGa_{1-x}As$ Epilayers

Composition x	Peak λ	Lifetime at 10K (μs) Short	Long
0	835	0.35	20.5
0.08	760	3.63	22.9
0.15	730	--	--
0.20	690	3.80	29.9
0.30	640	--	--
0.35	630	2.45	332
0.39	626	--	--
0.42	622	4.70	500
0.50	605	5.35	--

FIGURE CAPTIONS

Figure 1 a) Schematic of alternating thin layers of GaAs/AlGaAs in a MQWS.
b) Modulation of the bandstructure in a MQWS in (a)
c) Allowed $\Delta n=0$ transitions of MQWS.

Figure 2 Optical hole burning and fluorescence line narrowing of an inhomogeneously broadened spectroscopic line.

Figure 3 Wavelength shift with composition, x, of D-A recombination luminescence for Zn-doped $Al_xGa_{1-x}A_1$.

Figure 4 Showing the effects of inhomogeneous broadening on the decay profile of D-A emission in Zn-doped $Al_{0.35}Ga_{0.65}As$.

Figure 5 PL and PLE spectra of a MQWS consisting of 15 GaAs layers of thickness L_z = 6.5nm and barriers of width 175nm measured at 10K.

Figure 6 The PL peak energy plotted as a function of well width, L_z, on a log-log format. Samples KLB courtesy Philips Research Labs and samples Zn courtesy Dr J. Zavada.

Figure 7 Typical exciton photoluminescence from II-VI compound strained-layer superlattices measured at 90K.

Figure 8 Band structure of a typical type-II superlattice, with and without piezoelectric fields. The superlattice exciton recombination process is indicated.

Figure 9 Shape of le - hh transition in (a) samples KLB155 and (b) KLB219 measured in absorption (abs) and emission (em). The homogeneous profile is shown by the optical hole-burning line (OHB).

Figure 10 FLN spectra for a ZnS/CdSe superlattice.

Figure 11 Up-conversion in a III-V compound superlatice (KLB155)

Figure 12 Time integrated photoluminescence spectrum of typical CdS-CdSe superlattice.

Figure 13 Time-resolved photoluminescence, on a nanosecond timescale, of the intrinsic Stark superlattice CdS-CdSe. Spectra at 1ns, 2ns and 4ns delays show the relatively fast decay of the CdSe real-space-direct exciton near 700nm. The superlattice exciton, near 740nm, is relatively long-lived; it broadens and shifts at longer delays due to the intrinsic Stark effect.

Figure 14 Decay profile of exciton emission in CdS-CdSe superlattice.

Figure 15 Circularly polarized emission from GaAs/AlGaAs/ MQW (KLB219).

Figure 16a) Fluorescence due to exciton luminescence in a multiple single quantum well sample, GU154, of GaAs/$Al_{0.4}Ga_{0.6}As$. There is one luminescence signal for each well width of 4.0nm, 7.0nm and 110nm well.

b) Spectral variation in the ODCR signal detected as the change in fluorescence intensity, ΔI, induced by FIR laser radiation at 163μm in a magnetic field B=4.80T.

c) Change in fluorescence intensity from a QW with well width, L_z=7.0nm induced by FIR radiation of wavelength λ-163μm as a function of magnetic field.

SMS/DAJA45.7/2G.

References

1. C. Mailhiot and D. L. Smith, Phys. Rev. Lett. 58, 1264 (1987).
2. B. K. Laurich, D. L. Smith, K. lcess, C. G. Fonstad and C. Mailhiot, Superlattices and Microstructures 5, 341 (1989).
3. A. G. Cullis, P. W. Smith, P. J. Parbrook, B. Cockayne, P. J. Wright and G. M. Williams, Appl. Phys. Lett. 55, 2081, (1989).
4. T. Hakakawa, K. Takahashi, M. Kando, T. Suyama, C. Yamamoto and T. Hijikata, Phys. Rev. Lett. 60, 349 (1988).
5. M. P. Halsall, J. E. Nicholls, J. J. Davies, B. Cockayne, P. J. Wright and A. G. Cullis, Semicond. Sci. Technol. 3, 1126 (1988).
6. M. P. Halsall, J. E. Nicholls, J. J. Davies, B. Cockayne, P. J. Wright and A. G. Cullis, Superlattices and Microstructures 5, 189 (1989).
7. P. J. Wright, P. J. Parbrook, B. Cockayne, A. C. Jones, E. D. Orrell, K. P. O'Donnell and B. Henderson, J. Crystal Growth 94 (1989) 441.
8. A. C. Jones, S. A. Rushworth, P. J. Wright, B. Cockayne, P. O'Brien and J. R. Walsh, J. Crystal Growth 97 (1989) 537.
9. B. C. Cavenett and E. J. Pakulis, Phys. Rev. B 32, 8449, (1985).
10. M. P. Halsall, J. E. Nicholls, J. J. Davies, P. J. Wright and B. Cockayne, J. Cryst. Growth 102, (1990), in press.
11. J. Hegarty and M. D. Sturge, J. Opt. Soc. Am. B.2, 1143, (1985).
12. M. Kohlrausch, Ann. Phys. Leipzig 16, 102, (1873).
13. B. Henderson and G. F. Imbusch in *Opltical Spectroscopy of Inorganic Solids*, Chapter 7 (Oxford University Press, 1989).
14. K. P. O'Donnell, P. J. Parbrook, B. Hendrson, C. Trager-Cowan, X. Chen, F. Yang, M. P. Halsall, P. J. Wright and B. Cockayne, J. Cryst. Growth 102, (1990), in press.
15. T. Yokogawa, T. Saitoh and T. Narasawa, J. Cryst. Growth 102, (1990), in press.
16. G. Bastard, E. E. Mendez, L. L. Chang and L. Esaki, Phys. Rev. B28, 3241 (1983).
17. H. J. Polland, K. Kohler, L. Schultheis and J. Kuhl, Superlattices and Microstructures 2, 309 (1986).